Circulation Features of the Stratosphere Derived from Radiometric Temperature Measurements with the TIROS VII Satellite

JAMES S. KENNEDY[1]
U. S. Air Force, Air Weather Service, Washington, D.C.
AND WILLIAM NORDBERG
NASA, Goddard Space Flight Center, Greenbelt, Md.

(Manuscript received 19 April 1967, in revised form 8 August 1967)

ABSTRACT

Measurements of radiation emitted by atmospheric carbon dioxide at 15 μ were performed with the TIROS VII satellite. These measurements describe temperature patterns in the lower stratosphere. Temperature patterns covering a "quasi-global" zone (65N–65S) are investigated for the period June 1963–November 1964. The satellite observations reveal large-scale circulation features of the stratosphere, particularly during the late winter breakdown periods.

The salient feature in the Southern Hemisphere, during both late winters of 1963 and 1964, is the occurrence of a warm cell in the vicinity of Australia. This implies a deflection of the initially circumpolar vortex towards the eastern Pacific. In the Northern Hemisphere, winter is characterized by the well known warm cell over the Aleutian Islands with the vortex displaced towards the Atlantic. The Australian and North Pacific warm cells form the nucleus of the springtime warmings which then spread zonally over the entire Southern and Northern Hemispheres, respectively.

A quantitative Fourier analysis of the temperature variance along high latitude circles leads to the conclusion that there is considerable transport of ozone and heat by horizontal eddies in both hemispheres during winter. Disturbances in the zonal circulation during that period are predominantly of wave number one. During summer wave number zero prevails.

1. Introduction

Observations of global stratospheric temperature fields presented here are based on satellite measurements of the radiant emittance of the atmosphere in the spectral interval 14.8–15.5 μ. These measurements were obtained by TIROS VII continuously during June 1963 to November 1964. The radiometer consisted of a thermistor bolometer, filters, light gathering mirrors and lenses, and associated electronics. The instantaneous field of view was approximately 5°×5°. During a period of 12 hr, which corresponds to 14 consecutive orbits, the instrument scanned contiguously over the entire zone of the earth between 65N and 65S. Thus, ideally, radiation patterns over this "quasi global" zone could be mapped by the satellite every 12 hr. Practically, however, the time interval during which full coverage was achieved ranged over several days because measurements could not be transmitted to the ground for each and every full orbit. Also, the spatial resolution of the measurements presented here is considerably coarser than that ideally possible. Each instantaneous radiation measurement with a field of view 5°×5° corresponded to an area of 50×50 km on the surface of the earth. However, the radiometric accuracy of such a measurement when converted to equivalent black-body temperature was generally poorer than ±5C. Averaging many hunderd measurements over larger areas (5° latitude ×5° longitude near the equator and 2.5° latitude ×5° longitude near 60°) and time periods of 10 days resulted in nearly full coverage of the "quasi globe" with a relative accuracy of better than ±1C. There were two consistent gaps in the observations—one over the southern tip of South America, the other over Central Siberia (near 110E). These gaps were due to the fact that the orbits passing over these regions were always outside the communication range of data acquisition stations and observations over these regions could, therefore, never be transmitted to the ground. In the data presented here observations from adjacent areas were linearly extrapolated to cover these gaps.

Since the major features of stratospheric behavior are known to occur on a scale of thousands of kilometers (Teweles, 1963) and over periods of several weeks (Boville, 1960), the time and space averaging applied to our satellite measurements should not materially affect the information to be derived from these measurements. A detailed description of the instrument construction, the orbital geometry of TIROS VII, and the characteristics of the radiometer were published elsewhere (Staff Members, 1964). Preliminary results were discussed by Nordberg *et al.* (1965) and a complete pre-

[1] This work was performed while temporarily with the NASA Goddard Space Flight Center.

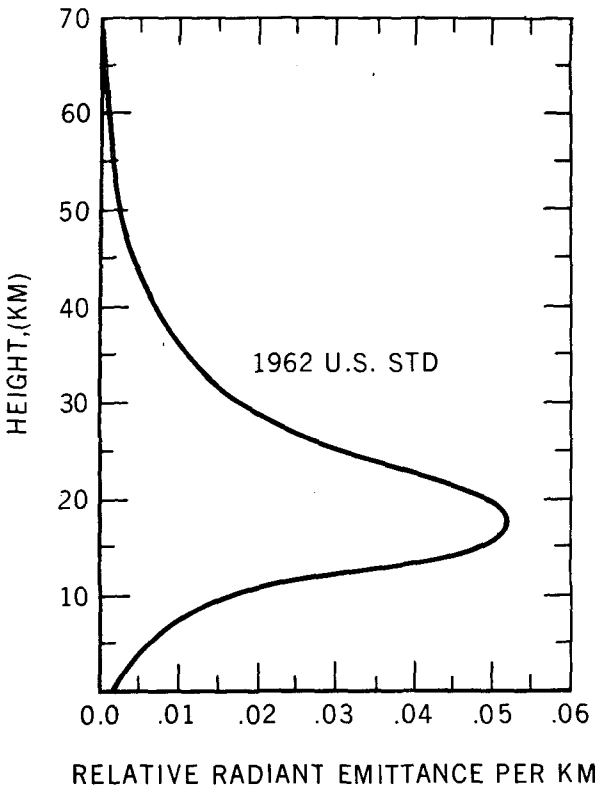

FIG. 1. Variation with height of computed ratio of radiant emittance for 1-km height intervals to total radiant emittance of the atmosphere, observable by TIROS VII in the 15-μ spectral region. Computation is based on an atmospheric temperature profile of the 1962 U. S. Standard Atmosphere.

sentation of the "quasi-global" temperature fields were given by Kennedy (1966).

2. Radiation measurements and stratospheric temperature patterns

The radiant emittances measured by the satellite sensor in this spectral interval (14.8—15.5 μ) are primarily due to thermal emission in the vibration-rotation band of carbon dioxide. It is assumed that carbon dioxide is distributed throughout the upper troposphere and stratosphere uniformly and at a constant mixing ratio. Also, assuming a typical temperature profile of the troposphere and stratosphere such as that given by the U. S. Standard Atmosphere (1962), one may compute for any given height interval in the atmosphere the radiant emittance which is transmitted to the satellite within this spectral interval. The result of such computation is shown, on a relative scale, in Fig. 1. The curve in Fig. 1 demonstrates that more than 90% of the total radiation sensed by the satellite is emitted by the atmosphere above 10 km. More than 70% of that total radiation is emitted at heights between 10 and 30 km. The weighting curve (Fig. 1) has a maximum near the 20-km level. Thus, if the measured radiant emittances are converted to equivalent black-body temperatures, they can be generally interpreted as atmospheric temperatures averaged over the height range from 10 to 30 km. The "weights" assigned to each height level in such an averaging process would correspond to the relative values given by the curve in Fig. 1. Equivalent black-body temperature is defined here as the temperature of an isothermal black body filling the field of view of the sensor (as in the laboratory calibration) which would cause the same response from the radiometer as does the general non-Planckian spectral distribution of the radiation emerging from the top of the atmosphere in the direction of the satellite.

Since a vertically weighted mean temperature does not easily fit into the framework of existing conventional measurements, the absolute values of equivalent black-body temperatures cannot be interpreted very readily as a meteorological measurement. At extratropical latitudes, where the atmospheric temperature between 10 and 30 km is quite constant, equivalent black-body temperatures correspond more closely to the actual temperature than in the tropics where the temperature varies greatly in this height range. Global, horizontal patterns of these temperatures are, however, very descriptive of large-scale circulation features in the lower stratosphere. All discussions of temperatures fields and circulation patterns derived from these measurements will therefore be based on the observed variation of equivalent black-body temperatures with time and space.

It must be noted that the weighting curve shown in Fig. 1 holds strictly only for the postulated temperature profile (U. S. Standard Atmosphere, 1962). A slightly altered weighting curve will result from other typical temperature profiles. However, it has been shown (Nordberg *et al.*, 1965) that variations in the weighting curves due to variations in the temperature profiles expected to exist at various latitudes and seasons are small. Fig. 1 also indicates that some radiation is observed from the lower atmosphere (5–10 km). In cases where an opaque cloud deck at the tropopause obscures the radiation from the underlying warmer atmosphere, derived equivalent black-body temperatures will be colder by about 5C than in cases where there are no clouds. This effect will be much more pronounced in the tropics than at high latitudes. But, except perhaps for the tropics, such temperature variation due to cloud cover will be minimized in the relatively large area and long time averages presented here. Thus, global patterns of observed equivalent black-body temperatures at 14.8–15.5 μ are highly indicative of the spatial and temporal variations of temperature in the lower and middle stratosphere.

3. Synoptic presentation of equivalent black-body temperature fields and inferred circulation

Figs. 2–5 are typical examples of the temperature patterns observed in the 60N to 60S "quasi-global"

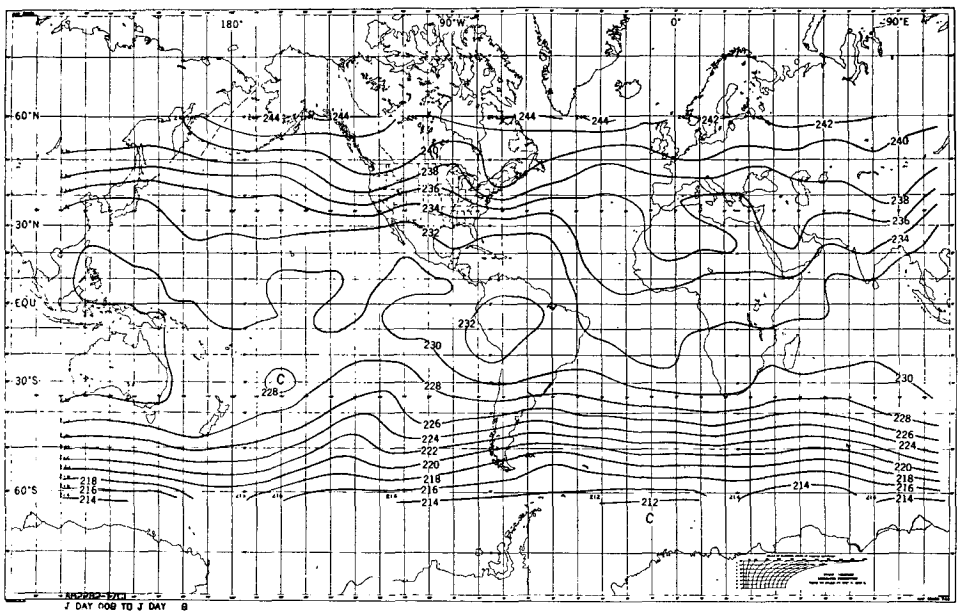

FIG. 2. Isotherms for average equivalent black-body temperatures derived from TIROS VII radiation observations during the period 19 June–28 June 1963. Numbers along isotherms refer to degrees Kelvin. Radiation observations were restricted to nadir angles 0–40°.

zone during the annual cycle from June 1963 to July 1964. Of some 70 such maps presented by Kennedy (1966) these were selected to illustrate how the satellite observations describe the morphology of the warm and cold air masses established in the respective summer and winter hemispheres. Especially in the vast oceanic and Southern Hemisphere areas, where observations were lacking thus far, the isotherm patterns shown in Figs. 2–5 can be used to obtain a better picture of the major circulation patterns in the stratosphere, the summer polar anticyclones and the winter polar vortices. These are quite apparent in Figs. 2 and 3 during the June 1963 and 1964 solstices. In both years the warm core is centered over the north polar cap, the cold core over the south polar cap. A significant deviation in the symmetry of the rather closely spaced isotherms around the south pole occurs over the central South Pacific. In 1963 (Fig. 2) a ridge of warm air (high pressure) extends to high latitudes southeast of Australia and over New Zealand while cold air (low pressure) pene-

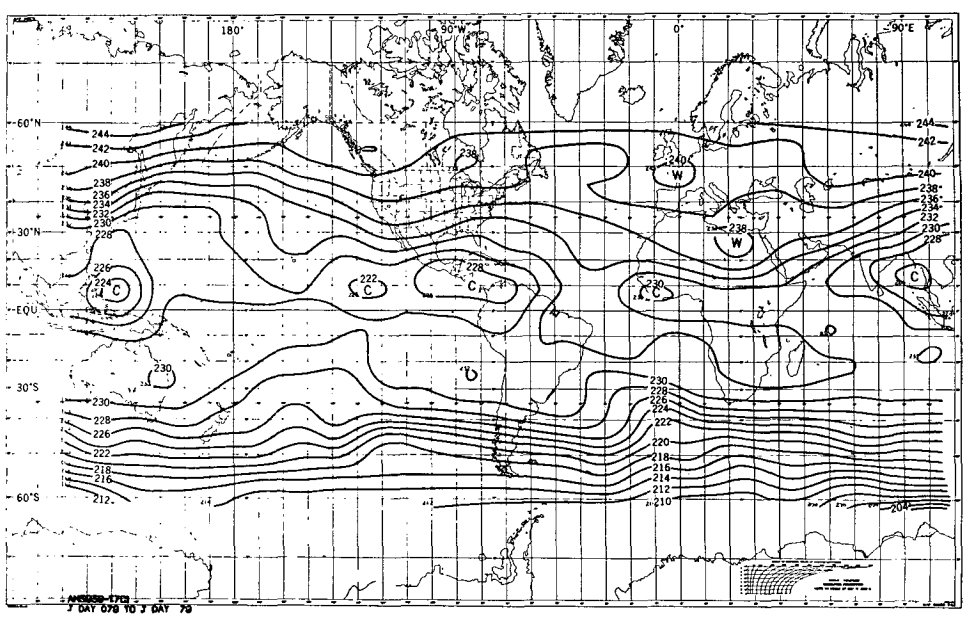

FIG. 3. Same as Fig. 2 for period 24 June–2 July 1964.

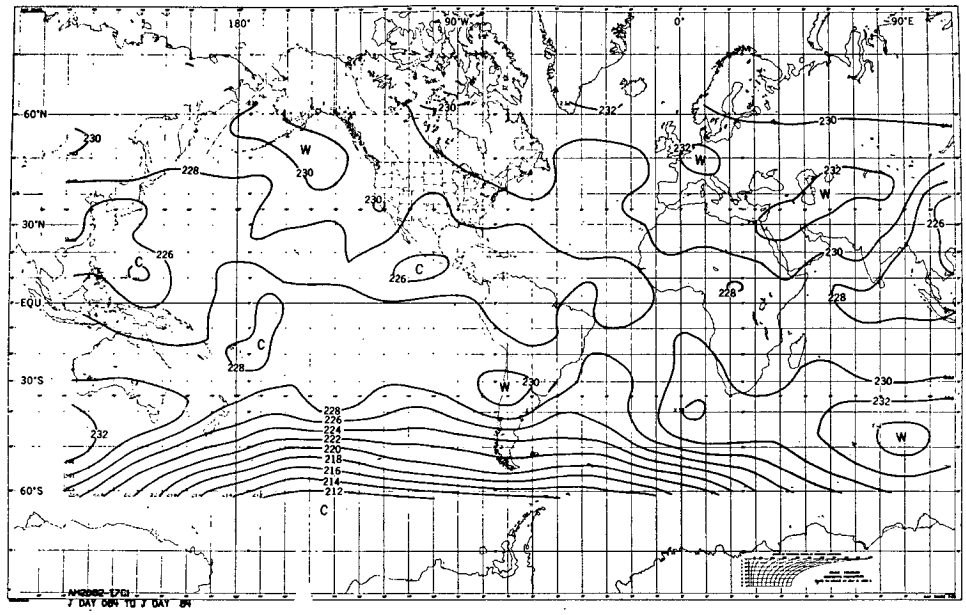

FIG. 4. Same as Fig. 2 for period 2–11 September 1963.

trates to low latitudes over the eastern Pacific Ocean, suggesting anticyclonic circulation over Australia. Differences of about 6C in equivalent black-body temperatures along latitude circles are observed between the western and eastern South Pacific. This asymmetry was observed during both the 1963 and 1964 (Fig. 3) Southern Hemisphere winters and was observed again with greater detail in the south polar region during 1966 with the Nimbus II satellite (Nordberg *et al.*, 1966). During 1963 the asymmetry becomes most pronounced in September (Fig. 4) when the vortex begins to break down. At that time the warm air ridge spreads considerably westward so that warm air occupies the entire southern Indian and Atlantic Oceans, while cold air still dominates the South Pacific. The equivalent black-body temperature difference between the Pacific and the Indian Oceans along 60S is almost 20C. This is greater than the 16C temperature difference between 30S and 60S during the June solstice (Fig. 2).

Northern Hemisphere isotherms display a familiar pattern (Fig. 5), well correlated with the circulation features already known from radiosonde observations

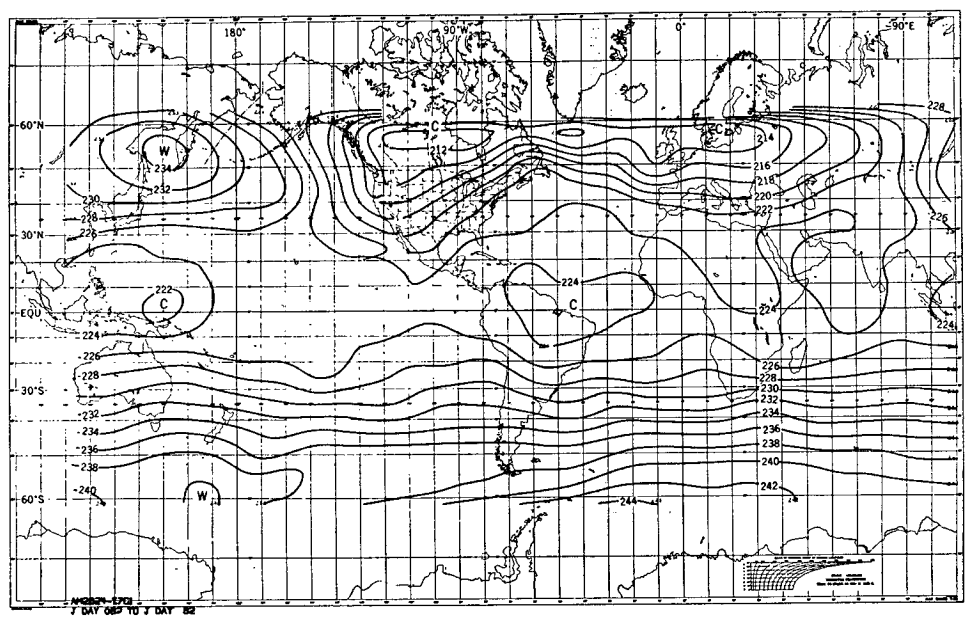

FIG. 5. Same as Fig. 2 for period 10–19 December 1963.

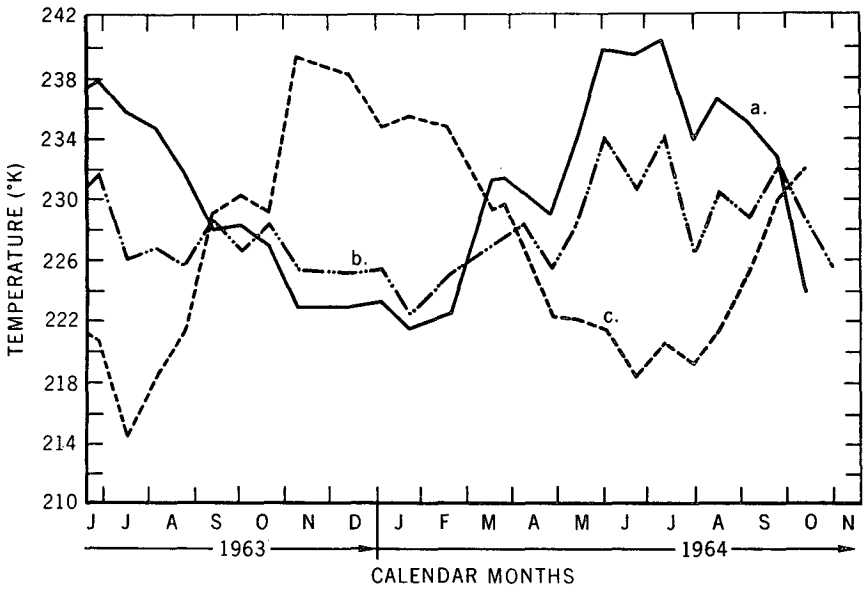

FIG. 6. Variations of average black-body temperatures derived from TIROS VII radiation observations with time for a., latitudes 40–65N, b., latitudes 30N–30S and c., 40–65S. Averages are for 10-day periods as shown in Figs. 2–5.

in this region. This correlation lends confidence to the application of satellite observations to infer circulation in areas where no conventional observations exist.

Temperatures in the tropics are considerably lower during December-January than they are during June-July (Fig. 6). There is an almost perfect phase relationship between the high latitude Northern Hemisphere and tropical temperature curves (shown as a and b of Fig. 6) and a 180° phase lag between the tropical and high latitude Southern Hemisphere temperature cycle (curves b and c). Note the almost identical zonal average temperatures at high northern and southern latitudes and in the tropics during the equinoxes. The difference in the amplitudes of the high latitude curves in the two hemispheres in winter indicates that the magnitude of the temperatures in the stratosphere are strongly influenced by probably both radiative exchange with the surface and lower atmosphere, and eddy transfer of energy within the stratosphere. The warm anticyclone over the North Pacific is obviously responsible for the fact that zonal average temperatures between 40–65N are 4–6C higher in December-January than corresponding temperatures between 40–65S during June-July. The almost equal amplitudes of the two high latitude curves in Fig. 6 during summer indicate that such effects are of lesser consequence in summer. A more detailed account of TIROS VII observations of stratospheric temperature patterns was given by Nordberg *et al.* (1965).

The complete and continuous maps of temperature fields presented by Kennedy (1966) permit an analysis of the development of the final stratospheric warmings in the Northern and Southern Hemispheres during March 1964 and September 1963, respectively. The essence of this analysis is illustrated in Figs. 7 and 8. The Northern Hemisphere warming of 1964 was clearly an example of the asymmetric or single source type as opposed to the symmetric or double source type (Wilson and Godson, 1963). The warm cell, located over the Kamchatka Peninsula in mid-February, spread eastward until early March, then expanded both eastward and westward and presumably poleward, displacing the rem-

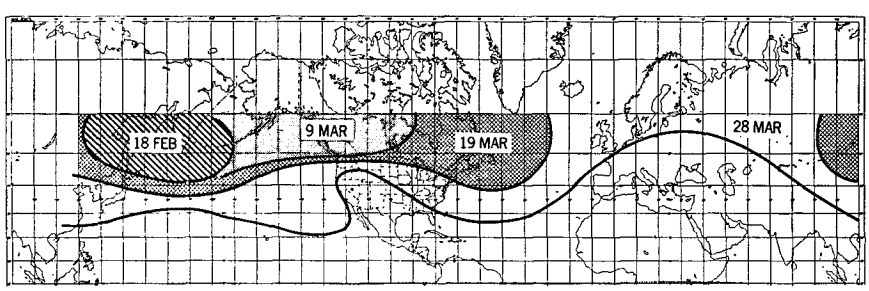

FIG. 7. Progression of the final warming in the Northern Hemisphere stratosphere in 1964. Solid lines indicate the 230K equivalent black-body isotherms for the dates shown.

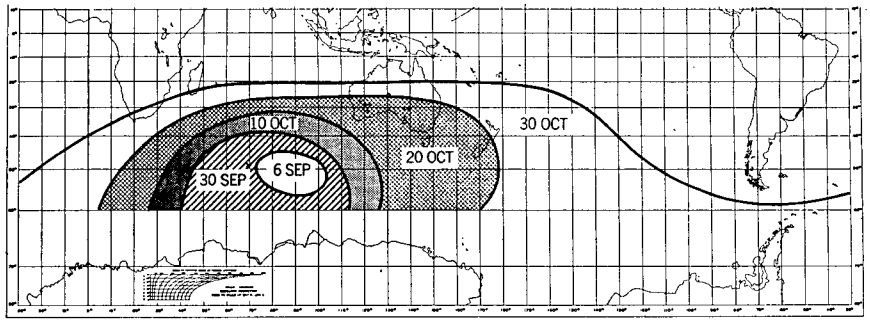

FIG. 8. Progression of the final warming in the Southern Hemisphere stratosphere in 1963. Solid lines indicate the 230K equivalent black-body isotherms for the dates shown.

nants of the cold polar vortex towards central Europe, where the cyclonic vortex dissipated in early April. The final warming occurred first over Canada, then Eastern Siberia, and last over Europe. The curves of Fig. 7 show that the entire transformation proceeded quite smoothly and steadily.

The final warming of the Southern Hemisphere (Fig. 8) was also of the single source type which Palmer and Taylor (1960) suggest is the rule in the Southern Hemisphere. Closed warm cells appeared south of Australia at latitude 40-50S in late August and shifted westward and southward in September to the south Central Indian Ocean. The warm cells increased in area in a series of surges, finally displacing the cold polar vortex towards South America in late October where dissipation occurred. The end of the final warming occurred well after the vernal equinox.

4. Horizontal eddy activity in both hemispheres illustrated by the variance in equivalent black-body temperatures

A more quantitative comparison of the Northern and Southern Hemisphere stratospheres may be made by examining the variance of temperature around latitude circles. Emphasis is placed on the behavior of the thermal patterns at the higher latitudes in each hemisphere primarily because of the more significant activity in these regions. The east-west temperature variance provides first a measure of the potential energy available for conversion into eddy kinetic energy (Lorenz, 1955). Secondly, it provides at least a qualitative estimate of the degree of horizontal eddy activity and the meridional flux of enthalpy by quasi-horizontal eddies. The actual transport depends, of course, on the covariance of temperature and the meridional wind component. However, a large variance of temperature makes possible a large wind temperature covariance and such large variances can be derived from the satellite-observed temperature patterns which are the only data at our disposal on a global scale. In this derivation we are obviously relying on previous studies of the stratosphere to judge the magnitude and even the sign of the wind-temperature covariance (Newell, 1965; Oort, 1963; Hare and Boville, 1966).

The temperature along a particular latitude is described by an equally spaced set of 72 values as a single valued periodic function. This function is expressed in a Fourier series of the form,

$$T(\lambda)=[T]+\sum_{n=1}^{36}(a_n\cos n\lambda+b_n\sin n\lambda), \tag{1}$$

where

$$a_n=\frac{1}{36}\sum_{i=1}^{72}T(\lambda_i)\cos(2\pi ni/72),$$

$$b_n=\frac{1}{36}\sum_{i=1}^{72}T(\lambda_i)\sin(2\pi ni/72),$$

and where T is the temperature (°K), λ the longitude, $[T]$ the zonal mean temperature, and n the zonal wave number. To express the thermal waves in terms of amplitude and phase, Eq. (1) may be rearranged to give

$$T(\lambda)=[T]+\sum_{n=1}^{36}c_n\cos(n\lambda-\phi_n), \tag{2}$$

where

$$c_n=(a_n^2+b_n^2)^{\frac{1}{2}},\quad n=1-35,$$

is the amplitude of the nth zonal harmonic, with $c_{36}=a_{36}/2$, and where $\phi_n=\arctan b_n/a_n$ is the phase of the nth zonal harmonic. The variance due to an individual harmonic is equal to $\frac{1}{2}c_n^2/2$ and the total variance of temperature σ_T^2 is given by

$$\sigma_T^2=\sum_{n=1}^{35}\tfrac{1}{2}c_n^2+c_{36}^2. \tag{3}$$

Use of the Fourier series makes possible the study of the development of significant harmonics in both amplitude and phase. The rationale for the expression of meteorological quantities in the domain of wave number is well covered by Saltzman (1957). The top curve in Fig. 9 is the zonal mean temperature difference between two northerly latitude circles and serves to indicate the progression of the seasons for the warm polar anticy-

clone of summer to the cold cyclonic vortex of winter. The center curves show the total temperature variance and that portion due to wave number one for a typical high latitude, 52.3N. The lower curve shows the longitudinal position lf the ridge of thermal wave number one for latitude 52.3N.

The variance curves show an absence of wave perturbations from the summer solstice to the autumnal equinox. Characteristically, the isotherms formed nearly concentric circles about the pole with the temperature increasing poleward. The phase of wave number one is included during the summer period only for purposes of continuity and has no physical significance as the amplitudes of all harmonics were below the noise level. At the autumnal equinox, the variance increased to a weak but significant level, then rose sharply in late November and maintained high values until the vernal equinox. The dashed curve shows that wave number one was the predominate mode throughout most of the winter. During the Northern Hemisphere winter of 1963-64, the thermal pattern was eccentric to the pole except for a brief period in late December when the thermal regime became bi-polar and thermal wave number two predominated.

One of the most remarkable features of the Northern Hemisphere winter stratosphere is illustrated by the curve showing the phase of thermal wave number one. The ridge of thermal wave number one became situated at about longitude 150E, at a time when the total variance and poleward temperature gradient were very weak, and remained quasi-stationary for the seven months period September 1963 to March 1964. It

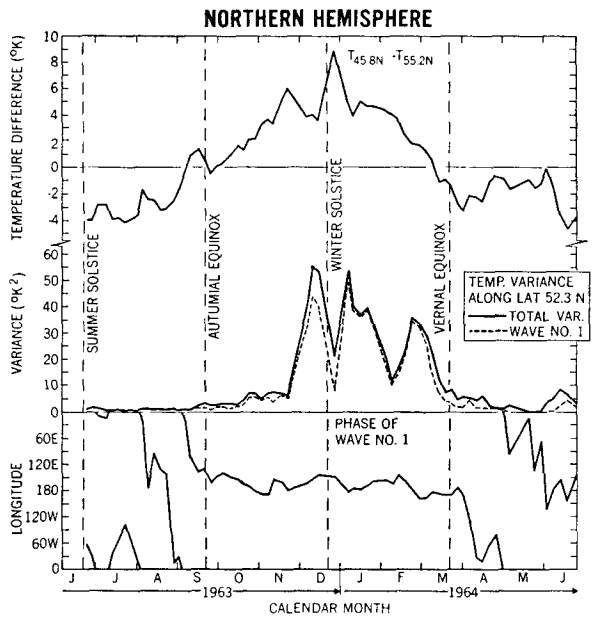

FIG. 9. Top: mean zonal equivalent black-body temperature difference between latitudes 45.8 and 55.2N; center: total equivalent black-body temperature variance (solid) and variance of first harmonic (dashed) along latitude 52.3N; bottom: longitudinal position of the ridge of the harmonic along latitude 52.3N.

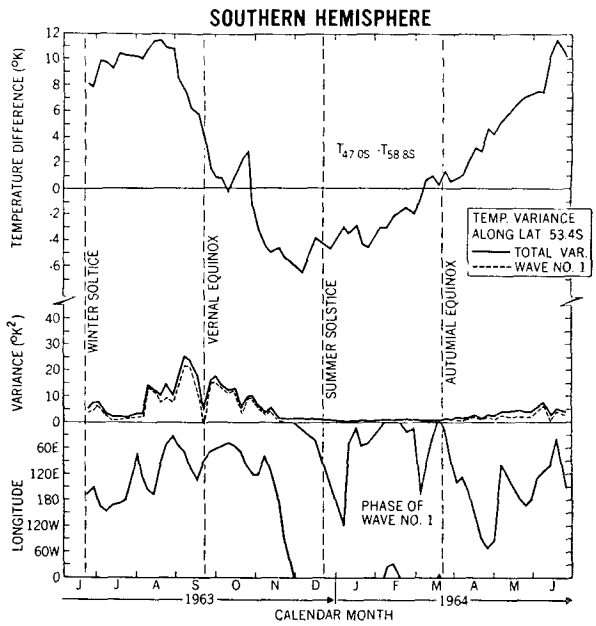

FIG. 10. Top: mean zonal equivalent black-body temperature difference between latitudes 47.0 and 58.8S; center: total equivalent black-body temperature variance (solid) and variance of first harmonic (dashed) along latitude 53.4S; bottom: longitudinal position of the ridge of the first harmonic along latitude 53.4S.

corresponds to the well known Aleutian anticyclone (Boville 1960).

Fig. 10 is the Southern Hemisphere counterpart to Fig. 9. The latitude selected was not quite the same as for the Northern Hemisphere because the basic grid was not centered at the equator, but the differences are minor. While we do not have appropriate wind data for the Southern Hemisphere, we shall assume that the temperature variance is indicative of the degree of horizontal eddy activity and of the poleward transport of heat and ozone.

The differences between the hemispheres are readily apparent. The markedly lesser eddy activity is to be expected due to the lack of continental forcing, but equally important is the different timing of the eddies. Whereas in the Northern Hemisphere the eddy activity was large a month before the winter solstice, the eddy activity in the Southern Hemisphere is negligible until over a month after the winter solstice. The lack of early winter eddy activity and related heat transport enables radiative effects to produce much colder winter temperatures in the Antarctic stratosphere (Godson, 1963) and the maximum poleward temperature gradient occurs at about the same time as the onset of eddy activity. This picture is again consistent with the observed ozone pattern. The Antarctic ozone is a minimum in winter (Hare and Boville, 1966) and begins to increase in eddy activity. The eddy activity continues for about two months after the vernal equinox, even after the springtime temperature gradient reversal (Fig. 10).

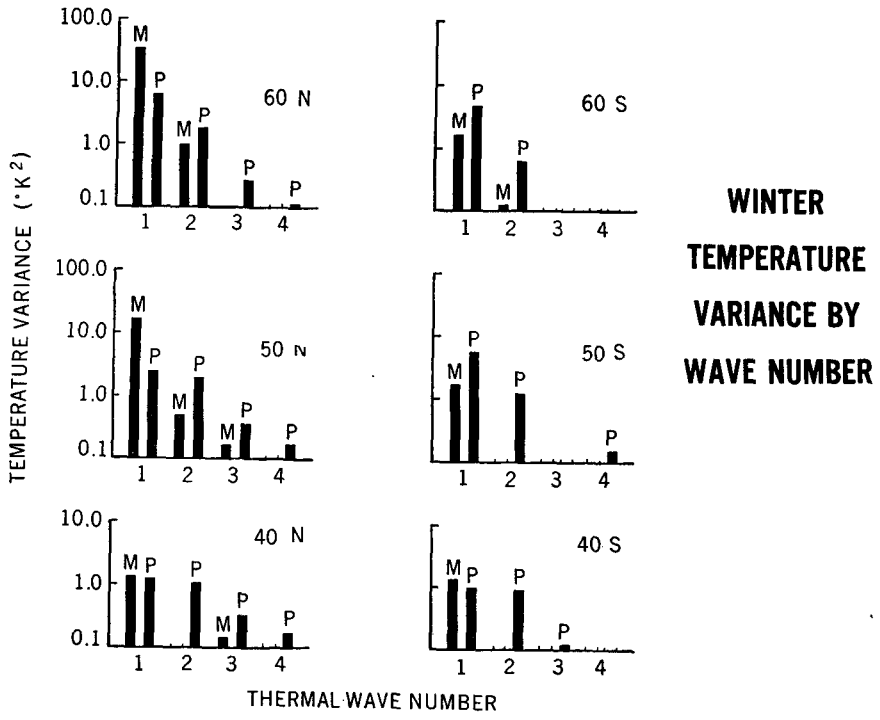

FIG. 11. Time-mean M and perturbation P components of the variance of the first four harmonics for the period December 1963—February 1964 in the Northern Hemisphere and June 1963—August 1963 in the Southern Hemisphere.

As in the Northern Hemisphere, the dashed curve in Fig. 10 shows that most of the variance is of wave number one. While wave number one in the Southern Hemisphere does not have the stability of its Northern Hemisphere counterpart, it is confined to a certain locality as shown by the phase curve of Fig. 10. The ridge of thermal wave number one originates south of Australia and travels spasmodically westward to the central South Indian Ocean. It is interesting to note that the warm ridge of wave number one remains in the approximate region where tropospheric cyclonic activity is a maximum (Lamb, 1959). The summer thermal patterns in the Southern Hemisphere is very similar to that of the Northern Hemisphere with no wave activity in evidence.

The basic differences between the winter circulations of the stratosphere in the two hemispheres are accentuated by examining the mean and perturbation components of the temperature variance (Fig. 11). The components are computed from seasonal averages of a_n and b_n of Eq. (1) and by expressing a_n and b_n as the sum of a time-mean and a perturbation component, *i.e.*,

$$\left.\begin{aligned} a_n &= \bar{a}_n + a_n' \\ b_n &= \bar{b}_n + b_n' \end{aligned}\right\}, \tag{4}$$

where an overbar indicates a seasonal time average and a prime indicates a deviation from the time average. The total variance due to an individual harmonic over a season, $\overline{c_n^2/2}$, can be expressed as

$$\begin{aligned} \overline{c_n^2/2} &= \tfrac{1}{2}(\overline{a_n^2}+\overline{b_n^2})+\tfrac{1}{2}\overline{[(a_n'^2)+(b_n'^2)]}, \\ &= \overline{c_n^2}/2+\overline{c_n'^2}/2, \end{aligned} \tag{5}$$

where $\overline{c_n^2}/2$ is the time-mean variance and $\overline{c_n'^2}/2$ is the perturbation variance, due to the nth harmonic.

Fig. 11 compares the results for the first four harmonics for the period December 1963 to February 1964 in the Northern Hemisphere and June to August 1963 in the the Southern Hemisphere, where M represents the time-mean values and P stands for the perturbation component. It may be seen that virtually all of the variance is explained by the first two harmonics in each hemisphere.

The time-mean values correspond to standing eddies, those that would appear on a mean seasonal chart. The perturbation values are only a rough approximation to transient eddies since they are derived from 10-day mean charts rather than instantaneous values. The perturbation values, however, should approximate the transient disturbances of a time scale greater than 10 days, which still include the major large-scale disturbances of the stratosphere.

The major difference between the hemispheres is found in the values of standing eddy number one at latitudes 50° and 60°. In the Northern Hemisphere due to the Aleutian anticyclone, the time-mean value of

thermal wave number one is about one order of magnitude greater than the perturbation component. In the Southern Hemisphere the perturbation component of wave number one is larger than the time-mean component. The appearance of a time-mean component of wave number one in the Southern Hemisphere, though small, is due to the warm portion of the wave remaining in one sector of the hemisphere throughout the winter. It is interesting that the perturbation components of waves one and two are similar in both hemispheres for equivalent latitudes, and at latitude 40°, the total wave structure is nearly indentical.

5. Conclusions

The observational results, which are limited to a temperature field smoothed with altitude as well as with time, and cover only a period of one seasonal cycle, do not permit an exhaustive analysis of climatological behavior of the stratosphere. They do illustrate, however, that satellite radiometry can provide a significant description of stratospheric behavior in the absence of other, more conventional, observations.

We conclude from the variations in the "quasi-global" patterns of equivalent black-body temperatures that the seasonal temperature cycle of the stratosphere in both hemispheres is exactly in phase with the variation of the declination of the sun. These temperature fields, especially the variance of temperature along high latitude circles, are indicative of large-scale horizontal eddies during winter in both hemispheres. The eddies, which are probably responsible for transporting heat and ozone to high latitudes, seem to develop in preferred locations around warm air cells over the Aleutian Islands and over Australia in the respective hemispheres. Wave number one dominates both of these eddies. The one in the Northern Hemisphere is considerably more intense and stationary than its Southern Hemisphere counterpart. In addition to differences in intensity and persistence there is another major difference between the eddy circulation in the two hemispheres. In both hemispheres eddy activity begins to increase at the autumnal equinox and intensifies abruptly about two months after that. In the Northern Hemisphere, however, this activity ceases abruptly just before the vernal equinox, while in the Southern Hemisphere it does not subside until about two months later. In both hemispheres large-scale eddy circulation is absent during the summer months. Temperatures in the tropics follow an annual variation which is in phase with the Northern Hemisphere cycle. Tropical temperatures are appreciably higher during June than during December.

REFERENCES

Boville, B. W., 1960: The Aleutian stratospheric anticyclone. *J. Meteor.*, **17**, 329–336.

Godson, W. L., 1963: A comparison of middle-stratospheric behavior in the Arctic and Antarctic with special reference to final warmings. *Meteor. Abhandl.*, **35**, 161–206.

Hare, F. K., and B. W. Boville, 1966: The polar circulations. The circulation in the stratosphere, mesosphere and lower thermosphere, World Meteorological Organization Tech. Note No. 70, Geneva, 43–78.

Kennedy, M. S., 1966: An atlas of stratospheric mean-isotherms derived from TIROS VII observations. NASA X-622-66-307, Goddard Space Flight Center, Greenbelt, Md.

Lamb, H. H., 1959: The southern westerlies: a preliminary survey; main characteristics and apparent associations. *Quart. J. Roy. Meteor. Soc.*, **85**, 1–23.

Lorenz, E. N., 1955: Available potential energy and the maintenance of the general circulation. Tellus, **7**, 157–167.

Newell, R. E., 1965: A review of studies of eddy fluxes in the stratosphere and mesosphere. Rept. No. 12, Planetary Circulation Project, Mass. Institute of Technology, 53 pp.

Nordberg, W., W. R. Bandeen, G. Warnecke and V. G. Kunde, 1965: Stratospheric temperature patterns based on radiometric measurements from the TIROS VII satellite. *Space Research*, Vol. 5, Amsterdam, North Holland Publishing Company, 783–809.

——, W. McCulloch, L. L. Foshee and W. R. Bandeen, 1966: Preliminary results from Nimbus II. *Bull. Amer. Meteor. Soc.*, **47**, 857–872.

Oort, A. H., 1963: On the energy cycle in the lower stratosphere. Rept. No. 9, Planetary Circulation Project, Mass. Institute of Technology, 122 pp.

Palmer, C. A., and R. C. Taylor, 1960: The vernal breakdown of the stratospheric cyclone over the South Pole. *J. Geophys. Res.*, **65**, 3319–3329.

Saltzman, B., 1957: Equations governing the energetics of the larger scales of atmospheric turbulence in the domain of wave number. *J. Meteor.*, **14**, 513–523.

Staff Members, 1964: *TIROS VII Radiation Data Catalog and User's Manual.* Vol. I, Goddard Space Flight Center, Greenbelt, Md., 256 pp.

Teweles, S., 1963: Spectral aspects of the stratospheric circulation during the IGY. Rept. No. 8, Planetary Circulation Project, Mass. Institute of Technology, 191 pp.

U. S. Standard Atmosphere, 1962. U. S. Government Printing Office, Washington D. C., 278 pp.

Wilson, C. V., and W. L. Godson, 1963: The structure of the arctic stratosphere over a 10 year period. *Quart. J. Roy. Meteor. Soc.*, **89**, 205–224.